Qiang Chen · George Chatzigeorgiou · Gilles Robert ·
Fodil Meraghni 🆔

Combination of mean-field micromechanics and cycle jump technique for cyclic response of PA66/GF composites with viscoelastic–viscoplastic and damage mechanisms

Abstract An accelerated micromechanics framework based on the extended Mori–Tanaka transformation field analysis (TFA) and cycle jump technique is proposed to predict the homogenized response of short glass fiber-reinforced polyamide 66 composites (PA66/GF) under a large number of loading cycles (> 100,000 cycles). The extended theory accounts for microscopic viscoelastic–viscoplastic and damage mechanisms, and realistic microstructures induced by the injection molding process. Toward this end, a number of training cycles are first conducted using the extended Mori–Tanaka TFA to obtain the global evolution functions of material state-dependent variables (*SDVs*) for each phase. These *SDVs* are extrapolated linearly to a certain jump length with the help of global evolution functions such that direct numerical simulation of the cycles during this interval can be skipped, leading to a large computational cost reduction. After the cycle jump, a set of complete cycles are performed based on the extrapolated *SDVs* using the Mori–Tanaka TFA simulation to re-establish the global evolution functions. The implementation of the cycle jump procedure is facilitated by introducing an extrapolation control function to allow adaptive jump size control as well as to minimize the extrapolating error. The capabilities of the extended theory with the cycle jump technique have been validated extensively vis-à-vis cycle-by-cycle benchmark calculations under various loading conditions. It has been further verified with the experimental results of actual PA66/GF composites under high-cycle loading beyond which the cycle-by-cycle simulations can achieve.

1 Introduction

During the past two decades, short fiber-reinforced polymer composites have been proved to be a good technological solution in various industry sectors such as automotive, aerospace, railways and electronics [1–3], in light of their excellent durability and lightness. These composite components are very often exposed to cyclic loading during service, which leads to a gradual degradation of the mechanical performances due to the microcrack initiation and coalescence, viscoplastic deformation and viscoelastic creep [4–6]. To make the best use of polymeric composites, it is vital to have a good understanding of the long-term behavior of such materials under arbitrary multiaxial loading conditions. However, the experimental work on composite materials under high-cycle fatigue loading is very costly and hence is limited to specific microstructures and loading configurations. This necessitates the development of efficient predictive tools that are capable of accurately estimating the response of polymeric composites taking into account the microstructural information and the dissipative mechanisms that take place during loading.

Q. Chen · G. Chatzigeorgiou · F. Meraghni (✉)
Arts Et Métiers Institute of Technology, CNRS, Université de Lorraine, LEM3-UMR7239, 57000 Metz, France
e-mail: fodil.meraghni@ensam.eu

G. Robert
Polytechnyl Sas - Domochemicals, 6919 Lyon, France

Simulating the nonlinear response of structures under a large number of cycles has been a bottleneck problem in the literature, especially when tens of thousands to millions of fatigue cycles are involved [7–9]. A simple load cycle is normally divided into many increments and iterations. This applies in particular to large-scale heterogeneous systems that contain many dissipative mechanisms, where the cycle-by-cycle simulations are barely affordable. An example in point is the injection-molded short glass fiber-reinforced polyamide 66 composites (PA66/GF), frequently used for automotive components subjected to cyclic loading. These composites have a specific skin–core–shell microstructure with short fibers distributed randomly in the laminate plane during the injection molding manufacturing process [10, 11]. Moreover, the PA66/GF composites exhibit remarkable time-dependent inelastic deformation due to the viscoelastic and viscoplastic mechanisms in the polyamide phase. Another important consideration that needs to be taken into account is the progressive matrix microcracking and interface debonding formed in this class of materials under a variety of loading and environmental conditions when the internal stress reaches the strength of the polyamide matrix or the interface [5, 12].

Homogenization theories are good predictive tools for the composite's macroscopic response using as information the response of the individual phases and the microstructures [13–17]. Homogenization techniques, in general, can be categorized into two broad categories, namely the full-field (i.e., periodic) and mean-field homogenization techniques. The periodic homogenization techniques, such as finite element [14, 18, 19] and finite volume-based approaches [20–22], are considered to be computation standards as they can take into account the detailed interaction of the microstructures. A major limitation of the periodic homogenization technique is that extensive mesh refinement is required in order to model the three-dimensional complex microstructures. For describing high-cycle fatigue behavior, the computation time of each loading cycle becomes essential for developing any micromechanics model. Therefore, the full-field homogenization methods are not feasible for high-cycle calculations of complex PA66/GF composites.

The mean-field homogenization techniques are analytical. Thus, they are extremely advantageous to periodic homogenization in terms of computation efficiency. These methods are accurate enough for the elastic moduli estimations, but appear to overestimate the stress–strain response when significant nonlinearities occur [23–25]. Our early attempts aimed at capturing the viscoelastic–viscoplastic deformation and the ductile damage of PA66/GF employ an extended micromechanics approach combining Mori–Tanaka with the transformation field analysis (TFA) [10, 26]. In this model, an interphase layer was introduced to correct the overestimation of stress–strain behavior in the nonlinear regime. Additionally, a phenomenological model consisting of four Kelvin–Voigt branches and a viscoplastic branch, formulated under the thermodynamics framework by Praud et al. [27], was utilized to describe the local deformation mechanisms of the polyamide phase. The interface debonding was described by the Weibull probabilistic density function to simulate the initiation and coalescence of the void-type discrete damage in the vicinity of the fiber/matrix interphase. It has been clearly revealed [10] that the extended Mori–Tanaka TFA approach for short fiber-reinforced composites with random fiber orientations, accounting for damage, viscoelastic and viscoplastic coupling mechanisms, is capable of reproducing the oligocyclic experimental response of PA66/GF composites with good accuracy. However, since a considerable amount of phases (for instance 36 orientations) needs to be considered in the extended Mori–Tanaka approach in order to properly capture the fiber orientation distribution, conducting the high-cycle analysis passing through every load cycle is still prohibited due to the high computation costs.

The cycle jump approach is a viable technique to circumvent the computational challenges posed by the cycle-by-cycle simulation. The cycle jump technique was originally proposed by Troschenko et al. [28] for the calculation of fatigue and life of crack-bearing structural elements, and further extended by Lesne and Savalle [29] for viscoplastic structure calculations. It has been adopted by numerous researchers for accelerated high-cycle computations [30–33]. For describing the high-cycle response of composite materials, Van Panpegem and coworkers [34, 35] have incorporated the cycle jump scheme into the continuum damage models to extrapolate the stiffness degradation of plain woven composites. Fish et al. [36] have introduced the cycle jump technique into a two-scale asymptotic homogenization approach to study the multiscale fatigue life of high-temperature ceramic matrix composites. Luders et al. [37] have developed an adaptive cycle jump method for micromechanical fatigue simulations of fiber-reinforced plastics. Sally et al. [38] have proposed an efficient computational strategy of cycle jumps dedicated to the fatigue of composite structures. Whatever the developed algorithm is, a common assumption adopted in various cycle jump techniques is that a single cycle is very short compared to the full cycle lifetime; therefore, the change of material states in one cycle is negligible compared to the change over the entire cycle lifetime. The general idea of the cycle jump method is then to avoid conducting cycle-by-cycle analysis with only a set of loading cycles simulated. At the interval where a large number of loading cycles can be skipped, the state-dependent variables (*SDVs*) necessary for obtaining

an appropriate homogenized behavior for any given load increments at each material phase are extrapolated to a certain jump length using the Euler forward approximation. The latter is based on the information of the simulated cycles before the attempted jumps. As a result, the computation time can be significantly reduced. Those extrapolated *SDVs* are subsequently utilized as initial conditions to perform a new set of control cycles after the cycle jumps.

In this study, a major interest is the implementation of the cycle jump procedure into the extended Mori—Tanaka TFA micromechanics method for the first time and employing the extended theory to predict the high-cycle response of PA66/GF composites under various loading conditions. This extension is based on performing Mori–Tanaka TFA simulation considering the viscoelastic–viscoplastic and damage mechanisms for a number of cycles to establish the global evolution functions of all the *SDVs*, extrapolating the *SDVs*, such as strain, stress, damage variables, viscoelastic and viscoplastic strains, which span over significant cycle lengths, and conducting a set of control cycles using the Mori–Tanaka TFA after the cycle jumps to obtain the updated global evolution functions. It should be noted that the determination of the proper cycle jump length is a key issue for the performance of the cycle jump technique since a high jump length reduces the computational cost, but simultaneously can increase the extrapolation error if not the numerical instability. Therefore, to enable efficient implementation of the cycle jump procedure, the extrapolation scheme with the control function proposed by Cojocaru and Karlsson [33] is adopted, which permits an automatic jump length and extrapolating error control over the cycle jump period. To the best knowledge of the authors, thus far, there has been no reported work of micromechanical simulations of the inelastic behavior of short glass fiber-reinforced polyamide composites with such complex behavior under high-cycle loading in the open literature. Such work is important to reduce the cost-prohibitive fatigue test of PA66/GF composites in automotive applications.

The remaining work is organized as follows: Sect. 2 recalls the theoretical framework of the extended Mori–Tanaka TFA approach with random fiber orientations and describes the implementation of the cycle jump algorithm into the extended Mori–Tanaka TFA micromechanics. Section 3 investigates the effect of cycle jump control parameters on the accuracy of the simulated response. Numerical verifications of the predictive capabilities of the cycle jump approach for simulating the inelastic response of short fiber-reinforced polyamide composites under high-cycle fatigue loading are also performed in this section. Comparisons of the extended cycle jump micromechanics simulations with the experimental results of actual composites under high-cycle loading are presented in Sect. 4. Limitations of the present work are discussed in Sect. 5. Section 6 draws the pertinent conclusions.

2 Theoretical development

2.1 Extended Mori–Tanaka TFA approach for randomly oriented short-fiber composites

In this section, the extended Mori–Tanaka TFA approach, developed by Chen et al. [10], accounting for the viscoelastic–viscoplastic and damage mechanisms is briefly recalled. For an N-orientation coated fiber-reinforced composite, as shown in Fig. 1, the averaged phase strain can be obtained using the transformation field analysis technique proposed by Dvorak [39] and Dvorak and Benveniste [40] as follows:

$$\boldsymbol{\varepsilon}_r^i = \mathbf{T}_r^i : \boldsymbol{\varepsilon}_0 + \mathbf{T}_{r0}^i : \boldsymbol{\varepsilon}_0^{in} + \mathbf{T}_{r1}^{i,i} : \boldsymbol{\varepsilon}_1^{in,i} + \mathbf{T}_{r2}^{i,i} : \boldsymbol{\varepsilon}_2^{in,i}, \tag{1}$$

where the superscripts $i = 1, ..., N$ are associated with variables in the i th fiber orientation while the subscripts $r = 1, 2$ represent the fiber and interphase phases, respectively. $\boldsymbol{\varepsilon}_0$ and $\boldsymbol{\varepsilon}_0^{in}$ denote the average matrix total strain and the matrix inelastic strain. $\boldsymbol{\varepsilon}_r^{in}(r = 1, 2)$ represents the inelastic strain of the r th phase. $\mathbf{T}_r^i$ ($r = 1$, 2) are the elastic interaction tensors of the i th fiber and i th coating, respectively. $\mathbf{T}_{rp}^i$ ($p = 0, 1, 2$) are the inelastic interaction tensors. For the expressions of these elastic and inelastic interaction tensors, the readers are referred to Chen et al. [10].

The homogenized strain for the overall composites is obtained as the weighted sum of the averaged strains over all the phases:

$$\overline{\boldsymbol{\varepsilon}} = c_0 \boldsymbol{\varepsilon}_0 + \sum_{i=1}^{N} \left[c_1^i \boldsymbol{\varepsilon}_1^i + c_2^i \boldsymbol{\varepsilon}_2^i \right], \tag{2}$$
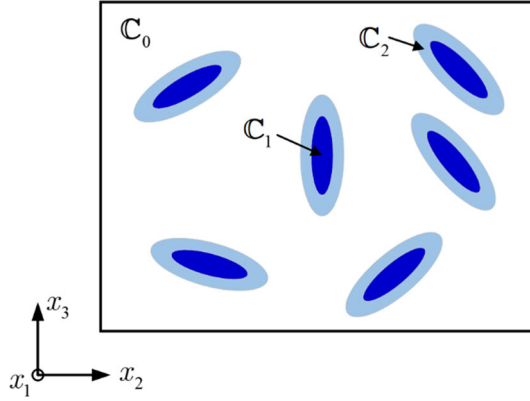
Fig. 1 Modified Mori–Tanaka scheme with multiorientation coated inclusions

where c_0 is the volume content of the matrix phase and c_r^i $(r = 1, 2)$ are the volume contents of the ith fiber and coating. Substituting Eq. (1) into Eq. (2) yields the homogenized strain in the following form:

$$\overline{\boldsymbol{\varepsilon}} = \left[c_0 \mathbf{I} + \sum_{i=1}^{N} \left[c_1^i \mathbf{T}_1^i + c_2^i \mathbf{T}_2^i \right] \right] : \boldsymbol{\varepsilon}_0 + \sum_{i=1}^{N} \left[c_1^i \mathbf{T}_{10}^i + c_2^i \mathbf{T}_{20}^i \right] : \boldsymbol{\varepsilon}_0^{in}$$
$$+ \sum_{i=1}^{N} \left[c_1^i \mathbf{T}_{11}^{i,i} + c_2^i \mathbf{T}_{21}^{i,i} \right] : \boldsymbol{\varepsilon}_1^{in,i} + \sum_{i=1}^{N} \left[c_1^i \mathbf{T}_{12}^{i,i} + c_2^i \mathbf{T}_{22}^{i,i} \right] : \boldsymbol{\varepsilon}_2^{in,i}. \tag{3}$$

To obtain the homogenized constitutive relations of the overall composites, the averaged strains in the matrix, fiber and coating are expressed in terms of the homogenized strain for the overall composites and inelastic strains of each phase as follows:

$$\boldsymbol{\varepsilon}_0 = \mathbf{A}_0 : \overline{\boldsymbol{\varepsilon}} + \mathbf{A}_{00} : \boldsymbol{\varepsilon}_0^{in} + \sum_{i=1}^{N} \mathbf{A}_{01}^i : \boldsymbol{\varepsilon}_1^{in,i} + \sum_{i=1}^{N} \mathbf{A}_{02}^i : \boldsymbol{\varepsilon}_2^{in,i},$$

$$\boldsymbol{\varepsilon}_1^i = \mathbf{A}_1^i : \overline{\boldsymbol{\varepsilon}} + \mathbf{A}_{10} : \boldsymbol{\varepsilon}_0^{in} + \sum_{j=1}^{N} \mathbf{A}_{11}^{j,i} : \boldsymbol{\varepsilon}_1^{in,j} + \sum_{j=1}^{N} \mathbf{A}_{12}^{j,i} : \boldsymbol{\varepsilon}_2^{in,j},$$

$$\boldsymbol{\varepsilon}_2^i = \mathbf{A}_2^i : \overline{\boldsymbol{\varepsilon}} + \mathbf{A}_{20} : \boldsymbol{\varepsilon}_0^{in} + \sum_{j=1}^{N} \mathbf{A}_{21}^{j,i} : \boldsymbol{\varepsilon}_1^{in,j} + \sum_{j=1}^{N} \mathbf{A}_{22}^{j,i} : \boldsymbol{\varepsilon}_2^{in,j}. \tag{4}$$

In the above equation, the various $\mathbf{A}_r$ and $\mathbf{A}_{rp}$ matrices denote the elastic and inelastic strain concentration tensors, respectively, which can be considered as the generalization of Eshelby's problem [41] for single inclusion to multi-inclusions interacting together in an average sense. The expressions for those concentration tensors revolve around the Eshelby tensors [41] that are expressed in terms of the matrix and interphase secant moduli, and the geometrical parameters of the inclusions. They can be evaluated analytically in the case of infinitely long cylindrical fibers or prolate spheroids embedded in an isotropic matrix [42]; otherwise, numerical technique developed by [43] should be employed.

It should be noted that just like all other mean-field micromechanics methods, the extended Mori–Tanaka TFA is based on the averaged field per phase. Therefore, the predictions of the overall inelastic behavior of a composite based on the extended Mori-Tanaka TFA method are considerably stiffer than the experimentally measured response or the response of full-field homogenization methods. The latter are considered to be computation standards in the literature. This was expected because the non-uniform stress/strain field concentration, predicted by the full-field homogenization, produces localized inelastic strains in the vicinity of the fibers. To account for the differences between the $\boldsymbol{\varepsilon}_0^{in}$ and $\boldsymbol{\varepsilon}_2^{in}$, a correction tensor $\mathbf{Y}$ is introduced as follows [24]:

$$\boldsymbol{\varepsilon}_2^{in} = \mathbf{Y} : \boldsymbol{\varepsilon}_0^{in}. \tag{5}$$

For a short glass fiber composite with fibers aligned in x_3 direction, the correction tensor $\mathbf{Y}$ takes the following form:

$$\mathbf{Y} = \begin{bmatrix} \gamma^N & 0 & 0 & 0 & 0 & 0 \\ 0 & \gamma^N & 0 & 0 & 0 & 0 \\ 0 & 0 & \gamma^L & 0 & 0 & 0 \\ 0 & 0 & 0 & \gamma^{ST} & 0 & 0 \\ 0 & 0 & 0 & 0 & \gamma^{SL} & 0 \\ 0 & 0 & 0 & 0 & 0 & \gamma^{SL} \end{bmatrix}, \tag{6}$$

where γ^N, γ^L, γ^{ST} and γ^{SL} represent the differences between the inelastic strains in the matrix and the inelastic strains in the virtual interphase in transverse normal, longitudinal, transverse shear and axial shear directions, respectively, which can be calibrated from the macroscopic experimental response or the full-field simulations. The averaged stress in each phase can be expressed as

$$\boldsymbol{\sigma}_1^i = \boldsymbol{C}_1^i : \left[\boldsymbol{\varepsilon}_1^i - \boldsymbol{\varepsilon}_1^{\mathrm{in},i} \right],$$
$$\boldsymbol{\sigma}_2^i = \boldsymbol{C}_2^i : \left[\boldsymbol{\varepsilon}_2^i - \boldsymbol{\varepsilon}_2^{\mathrm{in},i} \right] = \boldsymbol{C}_2^i : \left[\boldsymbol{\varepsilon}_2^i - \mathbf{Y} : \boldsymbol{\varepsilon}_0^{\mathrm{in}} \right],$$
$$\boldsymbol{\sigma}_0 = \boldsymbol{C}_0 : \left[\boldsymbol{\varepsilon}_0 - \boldsymbol{\varepsilon}_0^{\mathrm{in}} \right], \tag{7}$$

where $\boldsymbol{C}_0$ denotes the secant modulus of the matrix. $\boldsymbol{C}_1^i$ and $\boldsymbol{C}_2^i$ denote the secant moduli of the fiber and interphase in the i th direction, respectively. The computation of the inelastic strains and secant moduli depends on the chosen phase constitutive law, which will be given in Sect. 2.2.

Ultimately, the homogenized constitutive relation of the composites in the presence of damage and inelastic strains can be obtained as

$$\overline{\boldsymbol{\sigma}} = c_0 \boldsymbol{\sigma}_0 + \sum_{i=1}^{N} \left[c_1^i \boldsymbol{\sigma}_1^i + c_2^i \boldsymbol{\sigma}_2^i \right] = \boldsymbol{C}^* \overline{\boldsymbol{\varepsilon}} - \overline{\boldsymbol{\sigma}}^{\,\mathrm{in}}, \tag{8}$$

where $\overline{\boldsymbol{\sigma}}^{\,\mathrm{in}}$ denotes the homogenized inelastic stress. $\boldsymbol{C}^*$ is the effective secant modulus of the N-orientation coated short fiber-reinforced composite given by the following relation:

$$\boldsymbol{C}^* = c_0 \boldsymbol{C}_0 \mathbf{A}_0 + \sum_{i=1}^{N} \left[c_1^i \boldsymbol{C}_1^i : \mathbf{A}_1^i + c_2^i \boldsymbol{C}_2^i : \mathbf{A}_2^i \right]. \tag{9}$$

2.2 Constitutive laws for the matrix and interphase

The extended Mori–Tanaka TFA approach employs a phenomenological model consisting of four Kelvin–Voigt branches and a viscoplastic branch connected in series, formulated under the thermodynamics framework by Praud et al. [27], to characterize the local deformation mechanisms of the polyamide matrix phase. The damage mechanism in the matrix was described by the continuum damage mechanics theory based on the well-established principle of effective stress proposed by Lemaitre and Chaboche [44]. Under the thermodynamics framework, the Helmholtz free energy for the matrix medium can be expressed as

$$\rho \psi \left(\boldsymbol{\varepsilon}, \boldsymbol{\varepsilon}_{vi}, \boldsymbol{\varepsilon}_{vp}, p, d \right) = \frac{1}{2} \left(\boldsymbol{\varepsilon} - \sum_{i=1}^{N} \boldsymbol{\varepsilon}_{vi} - \boldsymbol{\varepsilon}_{vp} \right) : (1-d) \mathbf{C}_e : \left(\boldsymbol{\varepsilon} - \sum_{i=1}^{N} \boldsymbol{\varepsilon}_{vi} - \boldsymbol{\varepsilon}_{vp} \right)$$
$$+ \frac{1}{2} \sum_{i=1}^{N} \boldsymbol{\varepsilon}_{vi} : (1-d) \mathbf{C}_{vi} : \boldsymbol{\varepsilon}_{vi} + \int_0^p R(\xi) \, \mathrm{d}\xi, \tag{10}$$

where $\mathbf{C}_e$ (representing the initial matrix stiffness tensor $\mathbf{C}_0$) and $\mathbf{C}_{vi}$ denote the elastic stiffness tensor and the viscoelastic tensor of the i th branch, respectively. $\boldsymbol{\varepsilon}$, $\boldsymbol{\varepsilon}_{vi}$ and $\boldsymbol{\varepsilon}_{vp}$ are total, viscoelastic and viscoplastic strains, respectively. p is the viscoplastic scalar variable, and d denotes the ductile matrix damage variable represented as a scalar quantity. R is the hardening function. The evolution laws for the interval variables ($\boldsymbol{\varepsilon}_{vi}$,

$\mathbf{\varepsilon}_{vp}$, p and d) and their activation criteria are presented in Praud et al. [27]. Under the continuum damage mechanics theory, the secant modulus of the matrix in Eq. (7) can be expressed as: $\boldsymbol{C}_0 = (1 - d)\mathbf{C}_e$.

Additionally, virtual interphases are assumed to exist between the fibers and the matrix. They are occupied by the same polyamide material initially as in the matrix. The average viscoelastic–viscoplastic strains within the virtual interphases are directly linked to the matrix inelastic strains through Eq. (5). The damage mechanism in the interphase layers, however, is remarkably different from the matrix phase. While the damage in the matrix is characterized by gradual stiffness degradation that can be described by the continuum damage mechanics theory, the interphase debonding is catastrophic with the rapid occurrence and the coalescence of voids or defects [5, 12]. Therefore, the stiffness reduction $\mathbf{D}(\gamma_c)$ [10], induced by the void creation, is introduced to mimic the interphase debonding in the virtual coating layers.

$$\boldsymbol{C}_2(\gamma_c) = \mathbf{C}_0 - \mathbf{D}(\gamma_c) = (1 - \gamma_c)\mathbf{C}_0 : \mathbf{A}_m(\gamma_c) \tag{11}$$

In the above equation, $\mathbf{A}_m(\gamma_c)$ is the strain concentration tensor of the net matrix embedding voids and γ_c is the crack density [26, 45]. To naturally track the crack initiation and growth, the cumulative probability of the interphase crack density is described by the following Weibull-type probabilistic density function:

$$\gamma_c = \gamma_{\max}\left(1 - \exp\left(-\left[\frac{\langle \overline{\sigma}_2^{\text{eff}}\rangle}{\sigma_c}\right]^\kappa\right)\right), \tag{12}$$

where $\gamma_{\max}$ indicates the saturation limit of the microcrack density. $\overline{\sigma}_2^{eff}$ denotes the homogenized interphase effective stress. σ_c and κ are the Weibull parameters controlling how fast the interphase crack can grow.

2.3 Extended Mori–Tanaka TFA approach with controlled cycle jump: new developments

The extended Mori–Tanaka TFA approach with randomly oriented fibers can be implemented using the radial return mapping algorithm for the nonlinear micromechanics analysis [46, 47]. At each loading step, many loading increments and iterations are utilized to ensure the numerical convergence and stability of the nonlinear analysis. It should be noted that for an N-orientation coated fiber composite, the total number of interaction tensors is $8N$, while the total number of the concentration tensors is $4N^2 + 6N + 2$. These tensors need to be recalculated at each iteration of every loading increment. For describing high-cycle fatigue behavior, which is of particular interest in this work, the computation time becomes crucial for every single cycle simulation. The determination of these tensors in the Mori–Tanaka TFA approach with consideration of damage and various inelastic mechanisms relies on the numerical integration technique, hence consuming a considerable amount of computation resources and time.

To alleviate this issue, an accelerated Mori–Tanaka TFA scheme is introduced herein by assuming that there are no drastic variations in the state-dependent variables between the consecutive loading cycles under high-cycle loading. The general goal of the accelerated numerical scheme is to avoid simulating all individual cycles in a high-cycle analysis through the use of the "cycle jump" concept, therefore reducing significantly the need for repetitive evaluation of the interaction and concentration tensors. As illustrated in Fig. 2, the cycle jump procedure consists of the following steps:

Training cycle: a number of training cycles are conducted using the Mori–Tanaka TFA approach to obtain the global evolution functions of all the *SDV*s, which include the macroscopic stress, strain, inelastic strain, as well as viscoelastic strain, viscoplastic strain, damage variable in each phase;

Cycle jump: establishing the maximum common jump length of all the *SDVs* and extrapolating the *SDV*s based on the global evolution function to a certain jump length;

Control cycle: the extrapolated *SDVs* are used as the initial state for a new set of the Mori–Tanaka TFA micromechanics simulations after the cycle jump. The global evolution functions of all the *SDVs* are updated according to the control cycle analysis;

Repeat steps 2 and 3 to obtain the response till the desirable number of loading cycles or time.

Hereafter, the allowable jumped cycle in the extended Mori–Tanaka TFA analysis is determined based on the extrapolation scheme proposed by Cojocaru and Karlsson [33]. The latter permits automatic determination of the jump length during the cyclic loading. When a fast variation in the *SDVs* is observed, the extrapolation scheme automatically performs shorter or no jumps. Otherwise, a longer cycle jump will be conducted while the accelerated solutions remain close to the cycle-by-cycle simulation within a given tolerance.
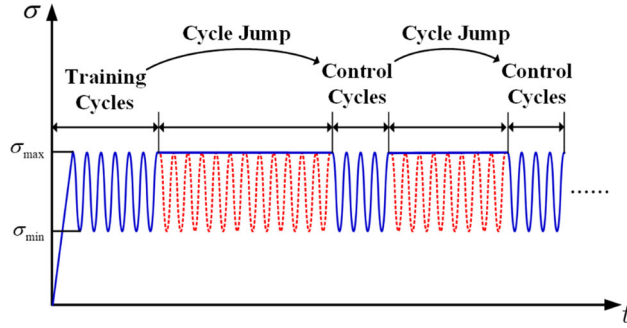
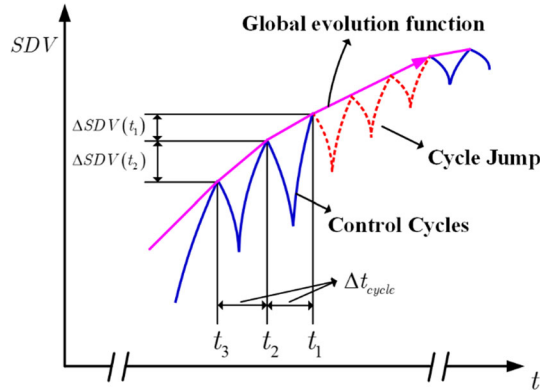**Fig. 2** Illustration of the cycle jump algorithm

Fig. 3 Approximation of the state-dependent variable evolution under cyclic loading

Let us assume that the solutions for at least three successive loading cycles have been obtained using the Mori–Tanaka TFA computation, as shown in Fig. 3. To establish the global evolution functions of state variables, the values for each SDV are extracted from the same relative position in time within each loading cycle, which are denoted by $SDV(t_1)$, $SDV(t_2)$ and $SDV(t_3)$. The differences in the state variables between the last two cycles are:

$$\Delta SDV(t_1) = SDV(t_1) - SDV(t_2), \tag{13}$$

$$\Delta SDV(t_2) = SDV(t_2) - SDV(t_3). \tag{14}$$

The corresponding slopes are expressed as:

$$s_{12}(t_1) = \frac{\Delta SDV(t_1)}{\Delta t_{\text{cycle}}}, \tag{15}$$

$$s_{23}(t_2) = \frac{\Delta SDV(t_2)}{\Delta t_{\text{cycle}}}, \tag{16}$$

where $\Delta t_{cycle} = t_1 - t_2 = t_2 - t_3$ represents the period of one cycle.

The allowable jump length Δt_{jump} for the designated SDV is given by the following criterion:

$$\frac{\left| s_p(t_1 + \Delta t_{\text{jump}}) - s_{12}(t_1) \right|}{|s_{12}(t_1)|} \leq q, \tag{17}$$

where q is a user-specified relative error greater than zero. Δt_{jump} is the time spanned by the cycle jump for the given SDV. $s_p(t_1 + \Delta t_{\text{jump}})$ indicates the predicted slope at the time after the cycle jump, which can be obtained by linear extrapolation as:

$$s_p(t_1 + \Delta t_{\text{jump}}) = s_{12}(t_1) + \frac{s_{12}(t_1) - s_{23}(t_2)}{\Delta t_{\text{cycle}}} \Delta t_{\text{jump}}. \tag{18}$$

Hence, Eq. (17) ensures that the predicted slope of each *SDV* at the time after the cycle jump is not too far beyond the known slopes before the attempted jump if a proper relative error q is prescribed.

Substituting Eq. (18) into Eq. (17) and considering that the time increment is non-negative yield the following expression for the determination of allowable jump length per *SDV*:

$$\Delta t_{\text{jump}} = q \, \Delta t_{\text{cycle}} \frac{|s_{12}(t_1)|}{|s_{12}(t_1) - s_{23}(t_1)|}. \tag{19}$$

It is worth noting that Eq. (19) only provides the allowed cycle jump length for one *SDV* at each phase. Nonetheless, the cycle jump lengths will not be necessarily the same for all the *SDVs* considered since the rate of changes of *SDVs* in short fiber-reinforced composites with viscoelastic–viscoplastic and damage mechanisms in different orientations can be drastically different. Thus, the common (or global) jump length $\Delta t_{\text{jump}}^{\text{common}}$ is obtained as the minimum of the computed allowed jump lengths for all the *SDVs*:

$$\Delta t_{\text{jump}}^{\text{common}} = \Delta t_{\text{cycle}} \left\lfloor \frac{\min\left\{\Delta t_{\text{jump}}\right\}}{\Delta t_{\text{cycle}}} \right\rfloor, \tag{20}$$

where $\lfloor \ \rfloor$ denotes the floor function.

Finally, the Heun integrator [33] is employed to perform the extrapolation of all the variables necessary for the next Mori–Tanaka TFA micromechanics analysis (control cycle):

$$SDV(t_1 + \Delta t_{\text{jump}}^{\text{common}}) = SDV(t_1) + \frac{1}{2}\left[s_{12}(t_1) + s_p(t_1 + \Delta t_{\text{jump}}^{\text{common}})\right]\Delta t_{\text{jump}}^{\text{common}}. \tag{21}$$

Substituting Eq. (18) into Eq. (21) yields the following formula for the computation of *SDVs* after the cycle jump:

$$SDV(t_1 + \Delta t_{\text{jump}}^{\text{common}}) = SDV(t_1) + s_{12}(t_1)\Delta t_{\text{jump}}^{\text{common}} + [s_{12}(t_1) - s_{23}(t_2)]\frac{\left(\Delta t_{\text{jump}}^{\text{common}}\right)^2}{2\Delta t_{\text{cycle}}}. \tag{22}$$

3 Numerical study

Having described the accelerated Mori–Tanaka TFA procedure, it is now of interest to test the accuracy of the cycle jump technique combined with the Mori–Tanaka TFA micromechanics vis-à-vis the cycle-by-cycle reference analysis and understand how various factors might influence the computation accuracy and efficiency.

The material system considered in this work is a thermoplastic short glass fiber-reinforced PA66/GF composite containing 30% fiber mass content, which corresponds to 15.5% fiber volume fraction. The average fiber aspect ratio is 22. Figure 4 shows the skin–shell–core microstructure of the PA66/GF composites, which has been frequently employed in a thin-plate structure of thermoplastic composites obtained by the injection molding manufacturing process. The skin–shell–core microstructure of the injection-molded PA66/GF composites was taken into account in an average sense by considering specific fiber orientation distribution following a density function. The latter is extracted from the micro-CT statistical measurement of an actual skin–shell–core microstructure in the entire through-thickness direction, as shown in Fig. 5. In the mean-field homogenization techniques, the reinforcement is taken into account through its volume fraction, orientation and aspect ratio. The actual position of fibers in the RVE is not considered in Eshelby-based micromechanics as in the Mori–Tanaka scheme.

The material parameters at room temperature and relative humidity of 50%, taken from Chen et al. [10], have been directly utilized in generating the results that follow (see Table 1). It should be noted that the damage-related parameter β is typically positive for metallic materials [48] for which these types of evolution laws were originally developed. The damage propagation in the case of positive values β occurs in a rather slow manner at the initial loading stage and propagates very fast at the latter loading stage. For thermoplastic polyamide, however, an inverse trend is usually experimentally observed [49], i.e., fast damage initiation followed by slow growth. This tendency can be well captured by setting negative values for the damage-related parameter β [50].
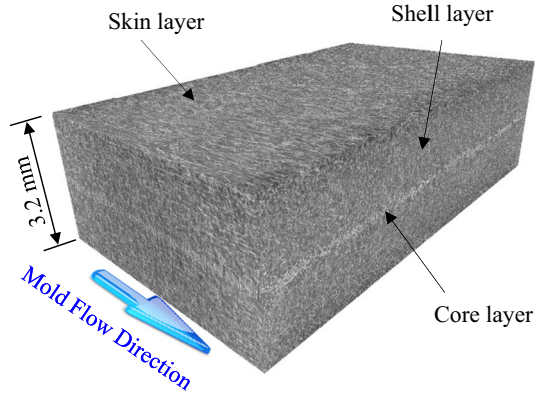
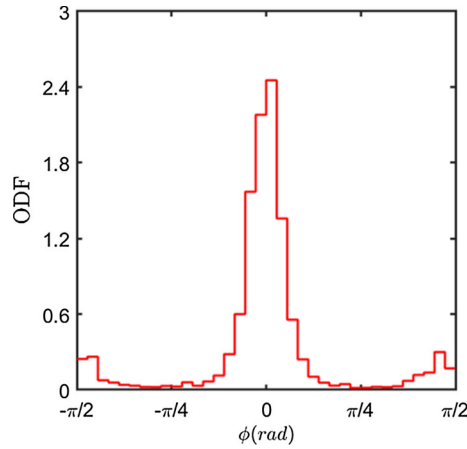**Fig. 4** Skin–shell–core microstructure in the through-thickness of PA66/GF composites

Fig. 5 Micro-CT statistical measurement fiber orientation density function

Table 1 Material parameters [10] used in the random Mori–Tanaka TFA simulation ($T = 23\,^\circ$ C, RH $= 50\%$)

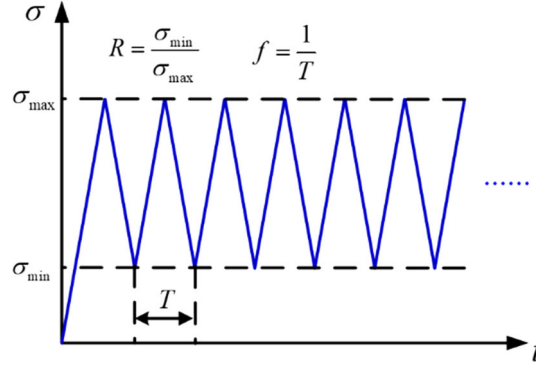|	Glass fiber	Polyamide interphase layer	Polyamide matrix
E	72.4 GPa	2731 MPa	2731 MPa
υ	0.22	0.3	0.3
E_{v1}		8766 MPa	8766 MPa
η_{v1}		1395 MPa s	1395 MPa s
E_{v2}		13,754 MPa	13,754 MPa
η_{v2}		165,601 MPa s	165,601 MPa s
E_{v3}		15,010 MPa	15,010 MPa
η_{v3}		457,955 MPa s	457,955 MPa s
E_{v4}		11,634 MPa	11,634 MPa
η_{v4}		1,307,516 MPa s	1,307,516 MPa s
R_0		4.86 MPa	4.86 MPa
K		1304.33 MPa	1304.33 MPa
n		0.674	0.674
H		47.35 MPa s	47.35 MPa s$^{\mathrm{m}}$
m		0.068	0.068
S			21.607
β			-1.105
γ^L		1	
γ^N		6	
γ^{ST}		2.64	
γ^{SL}		3.7	
$\gamma_{\max}$		0.99	
κ		0.62	
σ_c		55.20 MPa	

Fig. 6 Piecewise linear stress-controlled cyclic loading

3.1 Effect of cycle jump control parameter

The allowable jump length is determined by a user-defined parameter q which controls the difference of the predicted slope for each *SDV* the moment after the cycle jump with respect to the slope of the *SDV* before the attempted jump. The appropriate value for q needs to be determined by comparing the cycle-by-cycle simulation to the cycle jump simulation for a reasonable number of cycles. It should be also noted that the value of q for each *SDV* can be time-dependent, depending on the evolution mechanisms of each *SDV* during the cyclic loading. For the sake of simplicity, q is considered a constant value in this work. In the present study, the PA66/GF composites are subjected to piecewise linear stress-controlled cyclic loading with a frequency of f, as shown in Fig. 6. Before passing to the numerical study, let us first define the stress amplitude ratio in cyclic loading as

$$R = \sigma_{\min}/\sigma_{\max}, \tag{23}$$

where $\sigma_{\max}$ and $\sigma_{\min}$ represent the maximum and minimum stresses during the cyclic loading, respectively. Therefore, the cyclic loading history can be described by three parameters: R, $\sigma_{\max}$ and f.

First of all, the cycle jumps performed without the control parameter q are compared with cycle-by-cycle reference calculations. The accumulated effective plastic strain p and ductile damage d in the polyamide matrix are obtained for a PA66/GF composite, which is cut from a plate in 45° orientation with respect to the mold flow direction. Stress-controlled cyclic loading in the composite by the normal in-plane stress $\overline{\sigma}_{xx} \neq 0$ has been applied with $R = 0.1$, $\sigma_{\max} = 50$ MPa and frequency of 3 Hz. The global evolution function for each *SDV* is established based on 30 complete training cycles. The extrapolations are conducted repeatedly using Eq. (22) with two fixed jump lengths, namely 50 cycles and 100 cycles, respectively, which are followed by 6 complete control cycle simulations. For all the simulations, 3000 cycles were calculated to reach the target time of 1000 s. Comparing the differences between the cycle jump and cycle-by-cycle simulations in Fig. 7 clearly indicates that the effective plastic strains and ductile damage diverge immediately after the training cycles in the 100-cycle jump length case. The 50-cycle jump length produces stable response, but the solutions are visibly off from the reference solution. This suggests that the cycle jump without error control cannot guarantee that the correct values of the *SDVs* will be captured and hence may lead to unreliable solutions.

Next, the cycle jump simulations are obtained for four control parameters $q = 0.2, 0.5, 1.0, 1.5$. Cursory examination of Fig. 8 reveals that $q = 0.2$ and $q = 0.5$ predict indistinguishable results relative to the cycle-by-cycle reference calculations. Increasing q to 1.0 and 2.0 tends to slightly increase the differences between the cycle jump and the reference solutions, but does not produce a diverged response.

Comparisons of the computation time and the total number of jumped cycles for PA66/GF composites with 0°, 45° and 90° orientations between the cycle jump and cycle-by-cycle simulations are summarized in Table 2. The maximum stresses are 80 MPa, 50 MPa and 40 MPa, respectively, for 0°, 45° and 90° specimens. The stress amplitude ratio R and frequency f for the cyclic loading are 0.1 and 3 Hz for all the cases, respectively. It is observed the cycle jump procedure substantially reduces the number of cycles that need to be conducted relative to the cycle-by-cycle calculations. Increasing q can significantly increase the number of jumped cycles and hence an increase in computational efficiency. Hereafter, to balance the computation efficiency and accuracy, $q = 0.5$ will be employed unless otherwise stated.
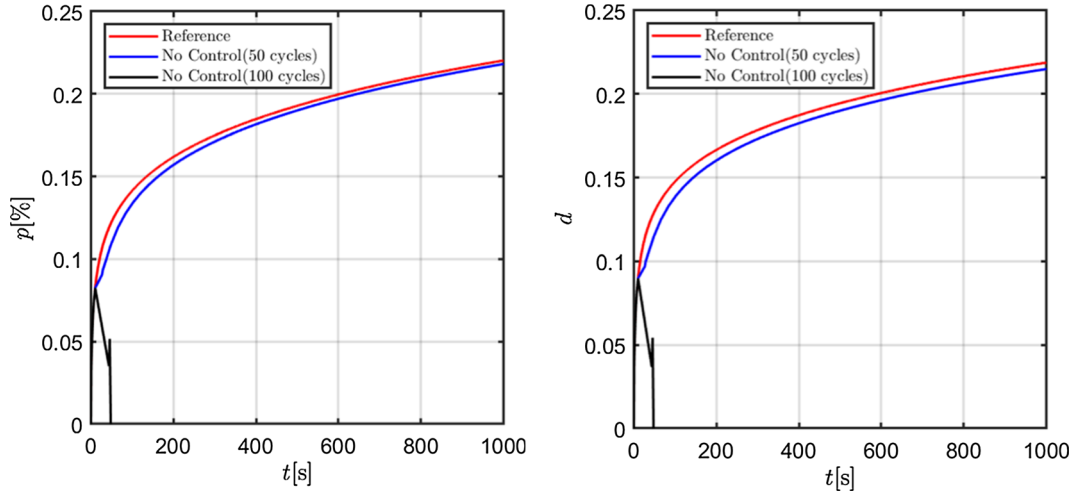
Fig. 7 Comparison of accumulated effective plastic strain and ductile damage in the matrix phase between cycle-by-cycle solution and cycle jump simulation without cycle control
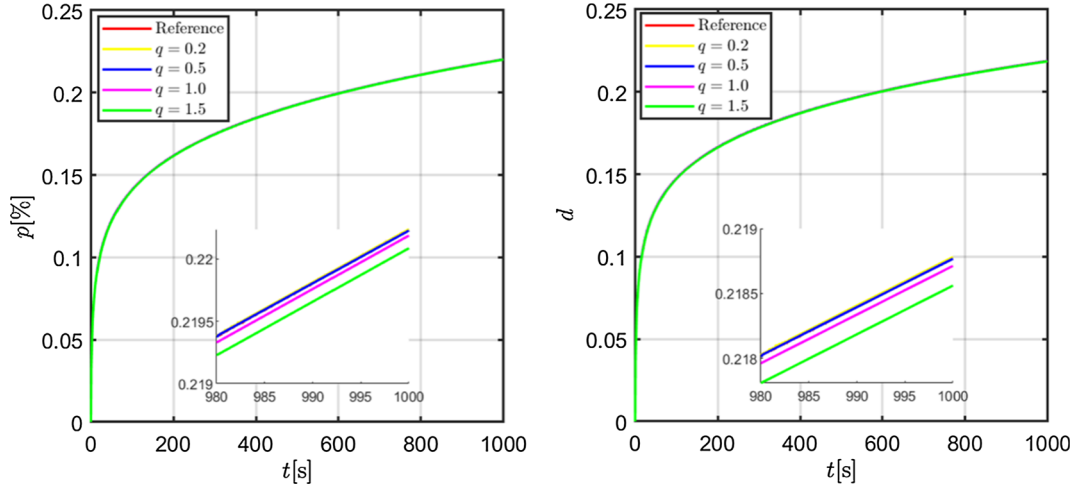

Fig. 8 Comparison of accumulated effective plastic strain and ductile damage in the matrix phase between cycle jump simulation and cycle-by-cycle reference solution for control parameters $q = 0.2, 0.5, 1.0, 1.5$

Table 2 Comparison of the computation time and total number of jumped cycles to reach 3000 cycles between the cycle jump simulation and cycle-by-cycle reference solution for control parameters $q = 0.2, 0.5, 1.0, 1.5$

Loading configuration	Control parameter	Number of jumped cycles	Computation time
0°	No jump	0	23 h 11 min
	$q = 0.2$	1629	10 h 53 min
	$q = 0.5$	2140	7 h 3 min
	$q = 1.0$	2393	5 h 10 min
	$q = 1.5$	2517	3 h 34 min
45°	No jump	0	20 h 48 min
	$q = 0.2$	1869	7 h 53 min
	$q = 0.5$	2259	5 h 31 min
	$q = 1.0$	2453	4 h 1 min
	$q = 1.5$	2543	3 h 20 min
90°	No jump	0	13 h 21 min
	$q = 0.2$	1714	5 h 54 min
	$q = 0.5$	2231	3 h 20 min
	$q = 1.0$	2464	2 h 16 min
	$q = 1.5$	2567	1 h 51 min

3.2 Comparisons of cycle-by-cycle and cycle jump simulations for different loading orientations

Figure 9 presents the comparison of the strain time response and strain envelope between cycle jump simulation and cycle-by-cycle reference solution for three PA66/GF specimens with different orientations, namely $\theta = 0°$, 45° and 90°. As observed, the cycle jump solutions show good accordance with the cycle-by-cycle reference solutions for all the loading cases. The employed extrapolation technique enables the automatic determination of a suitable jump length during the cyclic loading. As such, when there are fast variations in the *SDVs*, such as in the initial portion of loading cycles where significant nonlinearity occurs, the extended Mori–Tanaka TFA approach conducts shorter or no jumps. When the *SDVs* are stabilized, the extended Mori–Tanaka TFA approach performs longer jumps, thereby eliminating the need for extensive numerical computation during the period of the cycle jump.

Figure 10 shows the stress–strain response for the selected loading cycles for the above three orientations generated using the cycle jump procedure and the cycle-by-cycle reference solution. It is observed nearly identical results between the two solutions, providing good support for the cycle jump technique. Figure 11 presents the comparison of the effective plastic strain and the ductile damage in the matrix phase as a function of time generated by the cycle jump procedure and the cycle-by-cycle analysis. It is concluded that the control cycles between the jumps tend to bring back the solution to the reference results, indicating conducting more intermediate simulations will automatically decrease errors of the cycle jump simulations.

It should be mentioned that, thus far, the extended Mori–Tanaka TFA approach with cycle jump has been verified numerically against the cycle-by-cycle calculation. From the physical problem point of view, the cycle jump micromechanics approach developed in this work is a reliable technique as it gives satisfactory and consistent results compared to the reference solutions obtained without cycle jumps.

4 Experimental verification

In this section, the full potential of the extended Mori–Tanaka TFA approach with the cycle jump capability is further demonstrated by comparison with the experimental data under high-cycle loading conditions and extensively verified. These experiments were performed for PA66/GF specimens under stress-controlled loading with a frequency of 3 Hz. As mentioned by Arif et al. [5], the maximum strain rate is ranging between 0.07 and 0.2 s^{-1}. The specimens were placed in a climatic chamber with air containing 50% of relative humidity at 65°C. The conditioning process was carried on till all the specimens have a uniform water concentration (∼2.8%). The specimens were sealed prior to testing to maintain a controlled humidity.

Figures 12, 13 and 14 show the comparison of the maximum and minimum strains as a function of the loading cycle between the cycle jump predictions and experimental response for the PA66/GF composites loaded, respectively, in 0°, 45° and 90° orientations from the mold flow direction. The strain envelopes generated by cycle-by-cycle simulation up to 10 k loading cycles have also been enclosed in each figure for comparison. In the case of 0° specimens, two different stress magnitude ratios and maximum stresses, namely $R = 0.1$, $\sigma_{max} = 80$ MPa and $R = 0.3$, $\sigma_{max} = 90$ MPa, are applied. In the case of 45- and 90° specimens, several stress magnitude ratios and maximum stresses, namely $R = 0.1$, $\sigma_{max} = 50$ MPa; $R = 0.3$, $\sigma_{max} = 60$ MPa; $R = 0.5$, $\sigma_{max} = 70$ MPa and $R = 0.1$, $\sigma_{max} = 40$ MPa; $R = 0.3$, $\sigma_{max} = 54$ MPa, are performed, respectively. In general, the extended Mori–Tanaka TFA approach appears to reproduce the experimental response for the first 1000 cycles with sufficient accuracy. Particularly worthy of notice is the fact that the experimental response for the 45° specimens under $R = 0.1$, $\sigma_{max} = 50$ MPa and $R = 0.3$, $\sigma_{max} = 60$ MPa loading conditions are captured remarkably well. It should be also emphasized that the cycle-by-cycle and cycle jump simulations predict almost identical strain envelopes for every loading configuration, indicating the differences between the experimental and simulated results are not attributed to the cycle jump technique.

5 Remarks and limitations

Despite their successful applications in automotive industries, the characterization of nonlinear cyclic response of injection-molded short glass fiber polymer composites relies extensively on experiments. In addition to computational efficiency and implementability, the challenges in the modeling of PA66/GF composites include the need to take into account: (1) the skin–shell–core microstructures induced by the injection molding process; (2) the viscoelastic–viscoplastic response of the polymer matrix; and (3) damage mechanisms in constituent phases.
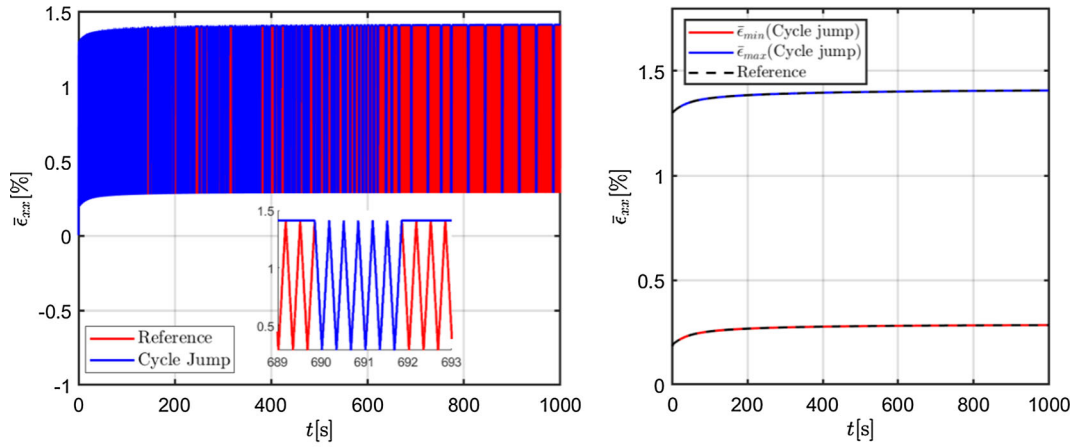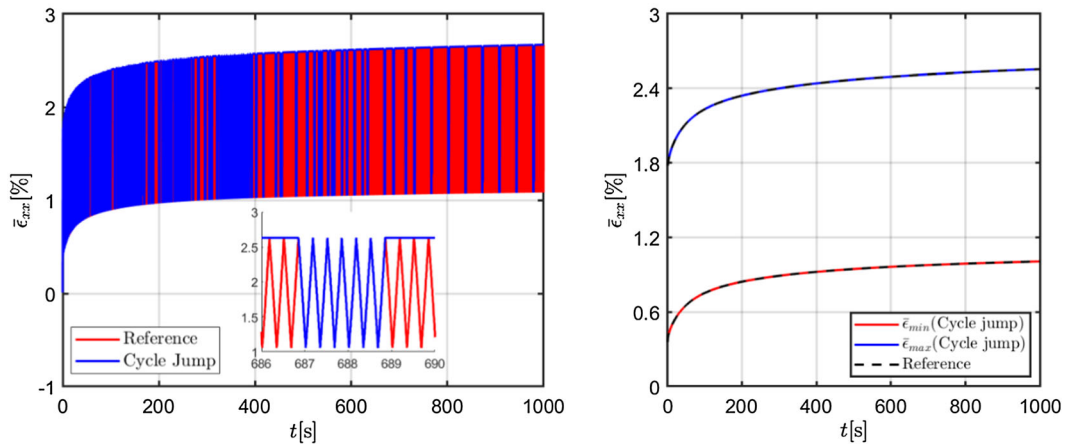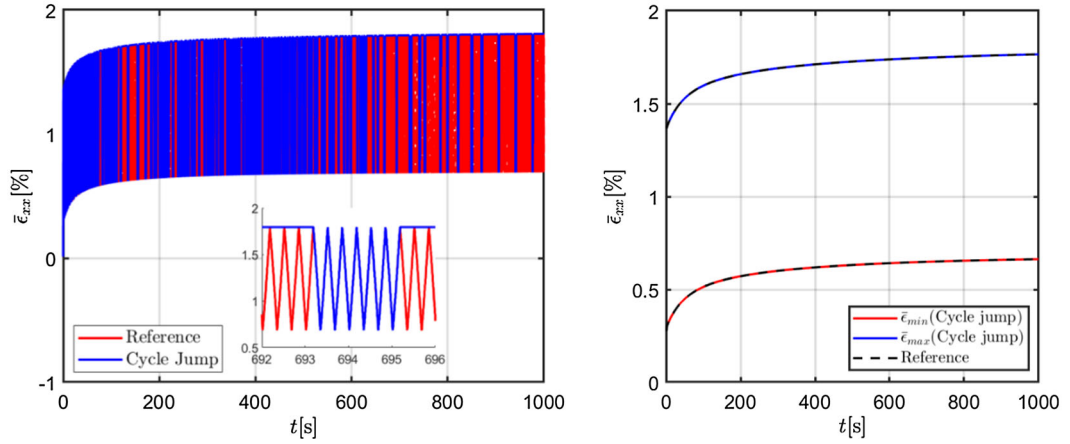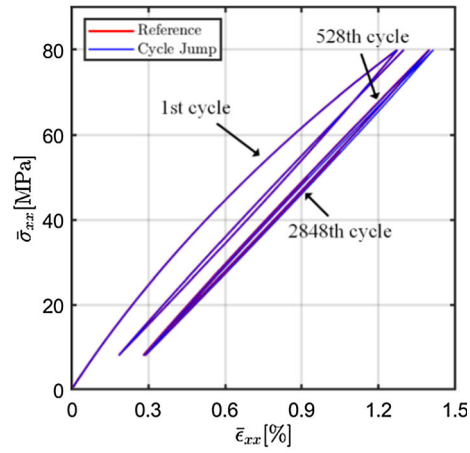
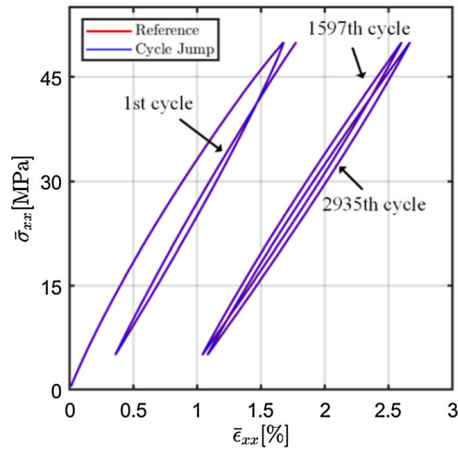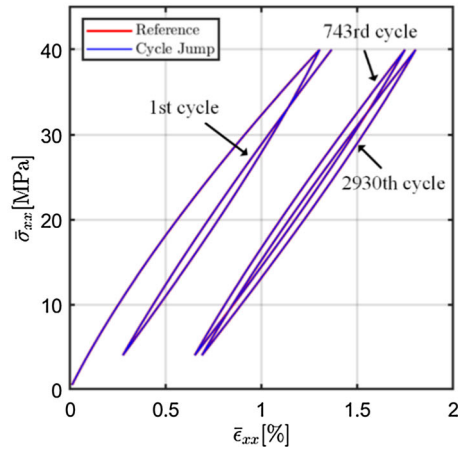**Fig. 9** Comparison of the differences in the strain time response (left) and strain envelope (right) between cycle jump simulation and cycle-by-cycle reference solution at three different loading configurations

Fig. 10 Comparison of stress–strain response between cycle jump simulation and cycle-by-cycle reference solution at the selected loading cycles for three different orientations
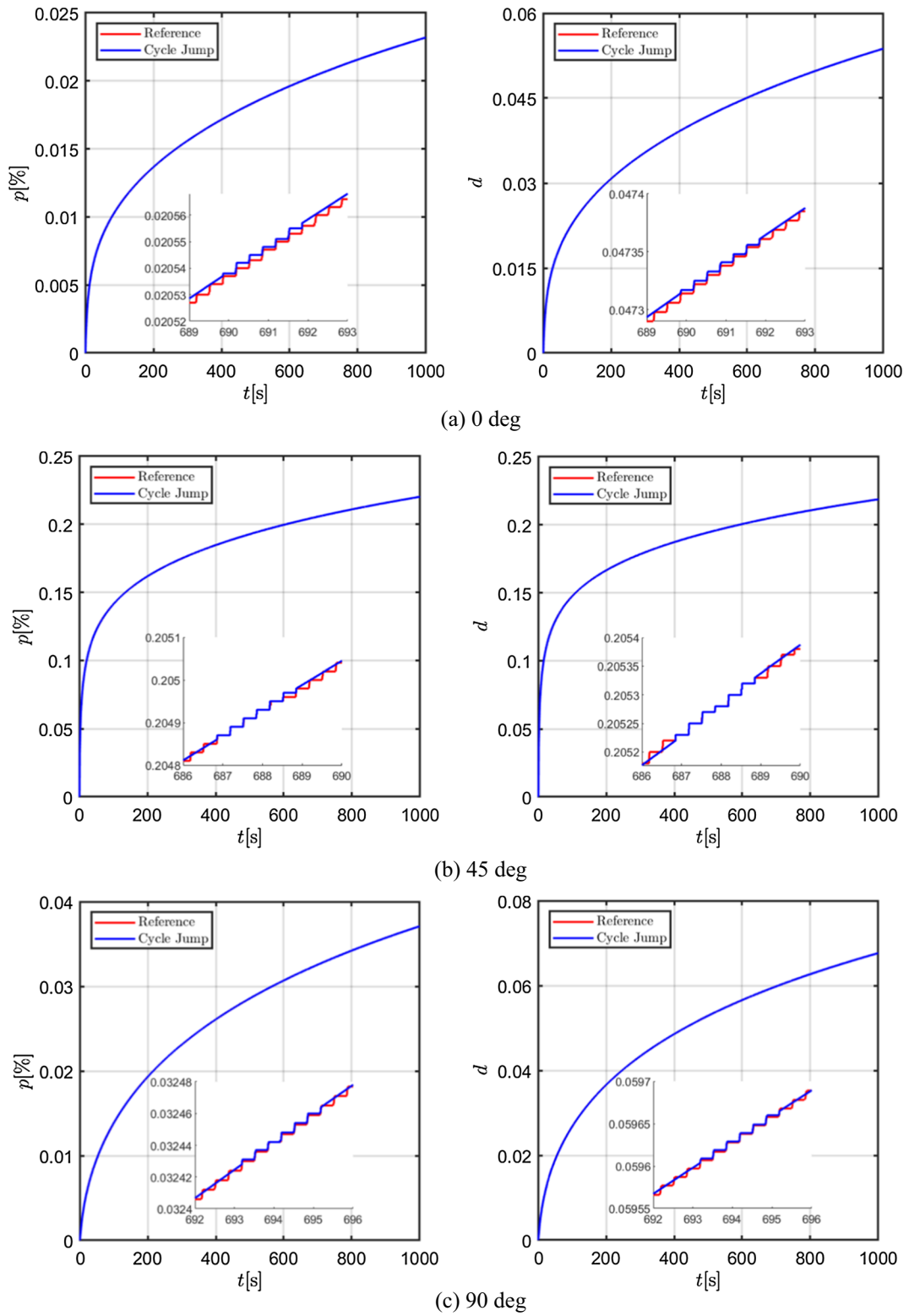
Fig. 11 Comparison of accumulated effective plastic strain and ductile damage in the matrix phase between cycle jump simulation and cycle-by-cycle reference solution for three different orientations
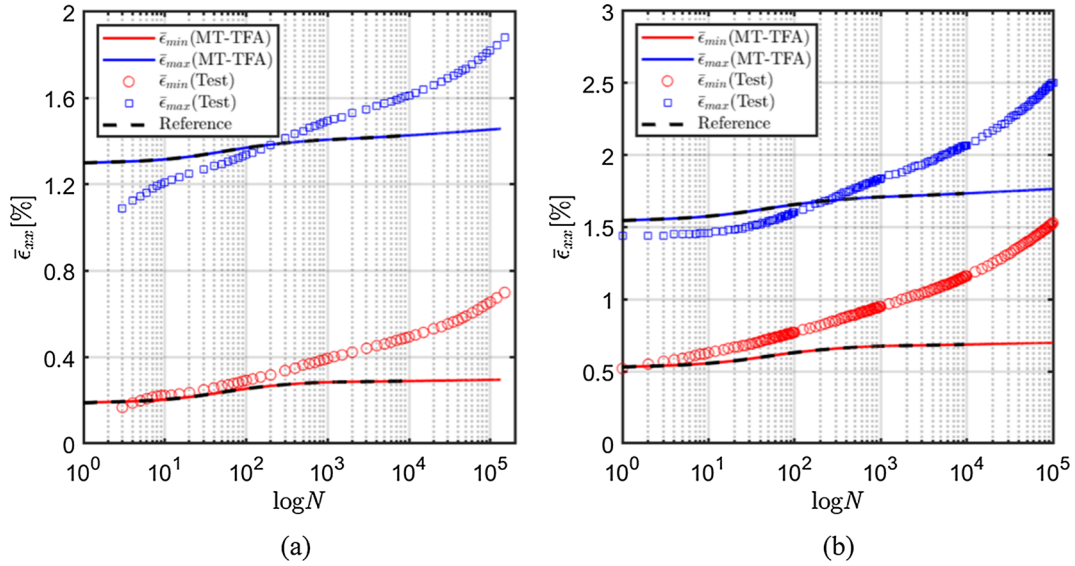
Fig. 12 Comparison of the maximum and minimum strains at each loading cycle for 0° PA66/GF30 composites under **a** $R = 0.1$, $\sigma_{\text{max}} = 80$ MPa and **b** $R = 0.3$, $\sigma_{\text{max}} = 90$ MPa

The present development of the extended Mori–Tanaka TFA framework with cycle jump technique attempts to shed light on efficiently simulating the high-cycle response of PA66/GF composites, accounting for the above-mentioned factors that may affect significantly the composite response for the first time. From the physical problem point of view, the cycle jump micromechanics approach developed in this work can be considered a reliable technique as it gives satisfactory and consistent results, but with reduced computational cost compared to the cycle-by-cycle reference solutions. An added advantage is that the proposed micromechanics model, contrary to phenomenological approaches, takes into account explicitly the microstructural characteristics and local constitutive laws.

The successful simulation of the experimental response of actual PA66/GF composites under different loading configurations demonstrates the potential of the proposed technique to predict the response of such composites under high-cycle loading. In general, the extended Mori–Tanaka TFA approach appears to reproduce the experimental response at the initial loading stages with sufficient accuracy for the 0° and 90° specimens and the entire loading stages for the 45° specimens. However, a close examination of Figs. 12, 13 and 14 also reveals that greater differences may occur at high loading cycles. This is particularly true for the specimen loaded with high mean stress, such as 45° specimen with $R = 0.5$, $\sigma_{\text{max}} = 70$ MPa and 90° specimens with $R = 0.3$, $\sigma_{\text{max}} = 54$ MPa. The reason for the observed discrepancies at the high-cycle range and high-mean-stress loading condition is several-fold. First of all, the parameters for the viscoelastic polyamide phase used in the extended Mori–Tanaka TFA simulations have been identified from experiments at short characteristic times and thus can only represent the short- or medium-term response. To capture long-term fatigue creep, more viscoelastic branches with higher characteristic times should be included in the polyamide constitutive model. Secondly, the experiment response manifests itself important "banana effect" characterized by larger hysteresis loops with increasing loading cycles, induced by the friction of the cracked phases combined with the viscoelasticity nature of the polyamide, which the extended Mori–Tanaka TFA approach does not capture. It should be emphasized that besides the microstructure variability induced by the injection process, the fatigue experiments exhibit significant discrepancies, especially for composites with random microstructures, at high loading cycles since they were not conducted in a constant environment. The relative humidity and temperature affecting the material response can evolve remarkably during the full cycling test due to several factors, among them energy dissipation and self-heating under the high-cycle range. As far, the extended micromechanics framework does not take into account the effect of temperature and humidity variations, and hence may further add to the differences between the experimental response and numerical simulation at the high-cycle range. It should be mentioned also that at the last stage of fatigue loading, fiber breakage may occur leading to the final macroscopic failure of the composite specimen [5, 12]. This mechanism is not taken into account in the present multiscale damage model either.
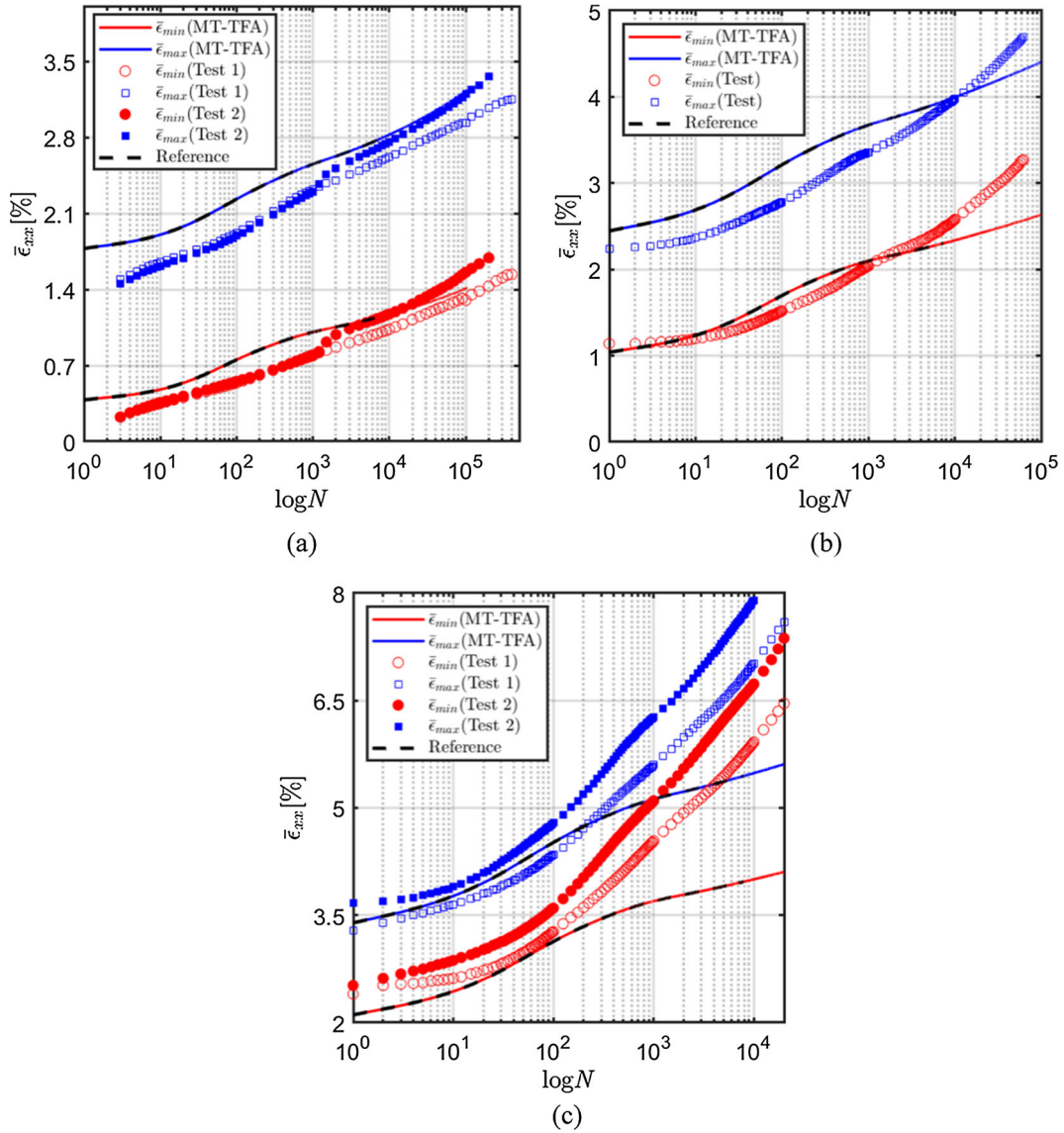
Fig. 13 Comparison of the maximum and minimum strains at each loading cycle for 45° PA66/GF30 composites under **a** $R = 0.1$, $\sigma_{\max} = 50$ MPa, **b** $R = 0.3$, $\sigma_{\max} = 60$ MPa and **c** $R = 0.5$, $\sigma_{\max} = 70$ MPa

6 Conclusion

A cycle jump-aided micromechanics methodology has been developed for simulating the high-cycle viscoelastic–viscoplastic response of short glass fiber-reinforced composites with ductile damage. The developed approach employs the previously developed extended Mori–Tanaka method and the transformation field analysis technique to obtain the homogenized behavior of composites with randomly oriented fibers. The response of the polyamide matrix is described by the viscoelastic–viscoplastic–ductile damage constitutive law. The extended theory circumvents the computation challenges imposed by the cycle-by-cycle simulation during the high-cycle loading. It simulates only a minimum number of cycles at the chosen time intervals while most of the cycles between these intervals are skipped using linear extrapolation. The implementation of the cycle jump technique is further facilitated by introducing an adaptive extrapolation scheme, which permits not only the automatic control of cycle jump length, but also good accuracy of the accelerated simulations.

Comparison of the cyclic response of randomly oriented short fiber-reinforced PA66/GF composites with 3 different off-axis orientations from the mold flow direction reveals excellent accordance of the cycle jump and the cycle-by-cycle simulations. The computational effort based on the former approach is drastically reduced
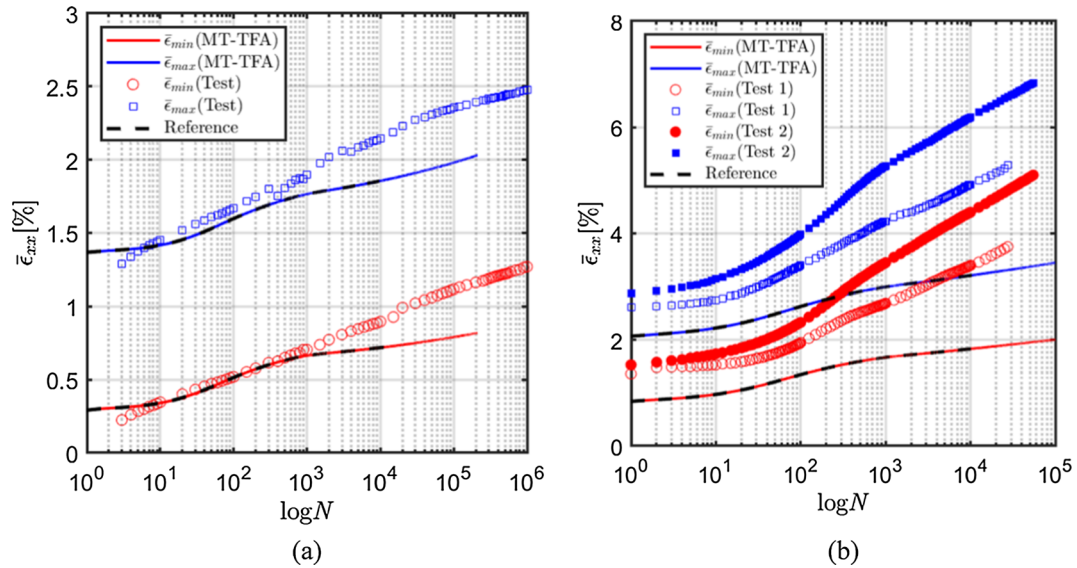
Fig. 14 Comparison of the maximum and minimum strains at each loading cycle for 90° PA66/GF30 composites under **a** $R = 0.1$, $\sigma_{\max} = 40$ MPa and **b** $R = 0.3$, $\sigma_{\max} = 54$ MPa

relative to the latter. The subsequent successful simulation of the experimental response of the PA66/GF composites with reasonable accuracy further demonstrates the potential of the developed cycle jump-aided micromechanics methodology in predicting the high-cycle (>100,000 cycles) response of the actual composites with complex microstructures and constitutive behaviors.

References

1. Gajek, S., Schneider, M., Böhlke, T.: An FE-DMN method for the multiscale analysis of thermomechanical composites. Comput. Mech. **69**, 1087–1113 (2022)
2. Dinzart, F., Torres-Costa, L.M., Sabar, H.: New micromechanical model in time domain for linear viscoelastic composites with ellipsoidal reinforcements. Acta Mech. **233**, 2009–2029 (2022)
3. Görthofer, J., Schneider, M., Hrymak, A., Böhlke, T.: A computational multiscale model for anisotropic failure of sheet molding compound composites. Compos. Struct. **288**, 115322 (2022)
4. Santharam, P., Marco, Y., Le Saux, V., Le Saux, M., Robert, G., Raoult, I., et al.: Fatigue criteria for short fiber-reinforced thermoplastic validated over various fiber orientations, load ratios and environmental conditions. Int. J. Fatigue **135**, 105574 (2020)
5. Arif, M.F., Saintier, N., Meraghni, F., Fitoussi, J., Chemisky, Y., Robert, G.: Multiscale fatigue damage characterization in short glass fiber reinforced polyamide-66. Compos. B Eng. **61**, 55–65 (2014)
6. Tu, W., Chen, Q.: Evolution of interfacial debonding of a unidirectional graphite/polyimide composite under off-axis loading. Eng. Fract. Mech. **230**, 106947 (2020)
7. Russo, A., Riccio, A., Sellitto, A.: A robust cumulative damage approach for the simulation of delamination under cyclic loading conditions. Compos. Struct. **281**, 114998 (2022)
8. Bian, L., Cheng, Y., Taheri, F.: Elasto-plastic analysis of critical fracture stress and fatigue fracture prediction. Acta Mech. **225**, 3059–3072 (2014)
9. Qin, D.-W., Ju, J.W., Zhang, K.-S., Li, Z.-S.: Inhomogeneous deformation growth of a metal under cyclic loading and its influence on fatigue. Acta Mech. **231**, 701–713 (2020)
10. Chen, Q., Chatzigeorgiou, G., Robert, G., Meraghni, F.: Viscoelastic-viscoplastic homogenization of short glass-fiber reinforced polyamide composites (PA66/GF) with progressive interphase and matrix damage: New developments and experimental validation. Mech. Mater. **164**, 104081 (2022)
11. Hessman, P.A., Riedel, T., Welschinger, F., Hornberger, K., Böhlke, T.: Microstructural analysis of short glass fiber reinforced thermoplastics based on x-ray micro-computed tomography. Compos. Sci. Technol. **183**, 107752 (2019)
12. Arif, M.F., Meraghni, F., Chemisky, Y., Despringre, N., Robert, G.: In situ damage mechanisms investigation of PA66/GF30 composite: effect of relative humidity. Compos. B Eng. **58**, 487–495 (2014)
13. Pindera, M.-J., Khatam, H., Drago, A.S., Bansal, Y.: Micromechanics of spatially uniform heterogeneous media: a critical review and emerging approaches. Compos. B Eng. **40**, 349–378 (2009)
14. Saeb, S., Steinmann, P., Javili, A.: Aspects of computational homogenization at finite deformations: a unifying review from Reuss' to Voigt's bound. Appl. Mech. Rev. **68**, 050801 (2016)
15. Chen, Q., Wang, G., Pindera, M.-J.: Homogenization and localization of nanoporous composites—a critical review and new developments. Compos. B Eng. **155**, 329–368 (2018)

16. He, Z.: Finite volume based asymptotic homogenization of viscoelastic unidirectional composites. Compos. Struct. **291**, 115601 (2022)
17. Schneider, M.: A review of nonlinear FFT-based computational homogenization methods. Acta Mech. **232**, 2051–2100 (2021)
18. Zhi, J., Poh, L.H., Tay, T.-E., Tan, V.B.C.: Direct FE2 modeling of heterogeneous materials with a micromorphic computational homogenization framework. Comput. Methods Appl. Mech. Eng. **393**, 114837 (2022)
19. Chen, Q., Chatzigeorgiou, G., Meraghni, F., Javili, A.: Homogenization of size-dependent multiphysics behavior of nanostructured piezoelectric composites with energetic surfaces. Eur. J. Mech. A. Solids **96**, 104731 (2022)
20. Chen, Q., Wang, G., Chen, X., Geng, J.: Finite-volume homogenization of elastic/viscoelastic periodic materials. Compos. Struct. **182**, 457–470 (2017)
21. He, Z., Pindera, M.-J.: Finite volume based asymptotic homogenization theory for periodic materials under anti-plane shear. Eur. J. Mech. A. Solids **85**, 104122 (2021)
22. Chen, Q., Pindera, M.-J.: Homogenization and localization of elastic-plastic nanoporous materials with Gurtin-Murdoch interfaces: an assessment of computational approaches. Int. J. Plast **124**, 42–70 (2020)
23. Hessman, P.A., Welschinger, F., Hornberger, K., Böhlke, T.: On mean field homogenization schemes for short fiber reinforced composites: unified formulation, application and benchmark. Int. J. Solids Struct. **230–231**, 111141 (2021)
24. Barral, M., Chatzigeorgiou, G., Meraghni, F., Léon, R.: Homogenization using modified Mori–Tanaka and TFA framework for elastoplastic-viscoelastic–viscoplastic composites: theory and numerical validation. Int. J. Plast **127**, 102632 (2020)
25. Haddad, M., Doghri, I., Pierard, O.: Viscoelastic-viscoplastic polymer composites: development and evaluation of two very dissimilar mean-field homogenization models. Int. J. Solids Struct. **236–237**, 111354 (2022)
26. Chen, Q., Chatzigeorgiou, G., Meraghni, F.: Extended mean-field homogenization of viscoelastic–viscoplastic polymer composites undergoing hybrid progressive degradation induced by interface debonding and matrix ductile damage. Int. J. Solids Struct. **210–211**, 1–17 (2021)
27. Praud, F., Chatzigeorgiou, G., Bikard, J., Meraghni, F.: Phenomenological multi-mechanisms constitutive modelling for thermoplastic polymers, implicit implementation and experimental validation. Mech. Mater. **114**, 9–29 (2017)
28. Troshchenko, V., Yasnii, P., Pokrovskii, V.: Calculation of fatigue and life of crack-bearing structural elements under cyclic load. Strength Mater. **14**, 1434–1439 (1982)
29. Lesne, P.-M., Savalle, S.: An efficient cycles jump technique for viscoplastic structure calculations involving large number of cycles. ONERA, TP no 1989–138. 1989:13.
30. Abdul-Latif, A., Razafindramary, D., Rakotoarisoa, J.C.: New hybrid cycle jump approach for predicting low-cycle fatigue behavior by a micromechanical model with the damage induced anisotropy concept. Int. J. Mech. Sci. **160**, 397–411 (2019)
31. Loew, P.J., Poh, L.H., Peters, B., Beex, L.A.A.: Accelerating fatigue simulations of a phase-field damage model for rubber. Comput. Methods Appl. Mech. Eng. **370**, 113247 (2020)
32. Titscher, T., Unger, J.F.: Efficient higher-order cycle jump integration of a continuum fatigue damage model. Int. J. Fatigue **141**, 105863 (2020)
33. Cojocaru, D., Karlsson, A.M.: A simple numerical method of cycle jumps for cyclically loaded structures. Int. J. Fatigue **28**, 1677–1689 (2006)
34. Van Paepegem, W., Degrieck, J., De Baets, P.: Finite element approach for modelling fatigue damage in fibre-reinforced composite materials. Compos. B Eng. **32**, 575–588 (2001)
35. Van Paepegem, W., Degrieck, J.: Fatigue degradation modelling of plain woven glass/epoxy composites. Compos. A Appl. Sci. Manuf. **32**, 1433–1441 (2001)
36. Fish, J., Bailakanavar, M., Powers, L., Cook, T.: Multiscale fatigue life prediction model for heterogeneous materials. Int. J. Numer. Meth. Eng. **91**, 1087–1104 (2012)
37. Lüders, C., Sinapius, M., Krause, D.: Adaptive cycle jump and limits of degradation in micromechanical fatigue simulations of fibre-reinforced plastics. Int. J. Damage Mech. **28**, 1523–1555 (2019)
38. Sally, O., Laurin, F., Julien, C., Desmorat, R., Bouillon, F.: An efficient computational strategy of cycle-jumps dedicated to fatigue of composite structures. Int. J. Fatigue **135**, 105500 (2020)
39. Dvorak, G.J.: Transformation field analysis of inelastic composite materials. Proc. R. Soc. Lond. A **437**, 311–327 (1992)
40. Dvorak, G.J., Benveniste, Y.: On transformation strains and uniform fields in multiphase elastic media. Proc. R. Soc. Lond. A **437**, 291–310 (1992)
41. Eshelby, J.D.: The determination of the elastic field of an ellipsoidal inclusion, and related problems. Proc. R. Soc. Lond. A **241**, 376–396 (1957)
42. Mura, T.: Mechanics of Elastic and Inelastic Solids. Micromechanics of Defects in Solids. Martinus Nijhoff Publishers, Dordrecht (1987)
43. Gavazzi, A., Lagoudas, D.: On the numerical evaluation of Eshelby's tensor and its application to elastoplastic fibrous composites. Comput. Mech. **7**, 13–19 (1990)
44. Lemaitre, J., Chaboche, J.-L.: Mechanics of Solid Materials. Cambridge University Press, Cambridge (1994)
45. Praud, F., Chatzigeorgiou, G., Chemisky, Y., Meraghni, F.: Hybrid micromechanical-phenomenological modelling of anisotropic damage and anelasticity induced by micro-cracks in unidirectional composites. Compos. Struct. **182**, 223–236 (2017)
46. Chatzigeorgiou, G., Charalambakis, N., Chemisky, Y., Meraghni, F.: Computational Methods. In: Chatzigeorgiou, G., Charalambakis, N., Chemisky, Y., Meraghni, F. (eds.) Thermomechanical Behavior of Dissipative Composite Materials, pp. 89–116. Elsevier, Amsterdam (2017)
47. Chatzigeorgiou, G., Meraghni, F., Charalambakis, N.: Chapter 12—Nonlinear composites. In: Chatzigeorgiou, G., Meraghni, F., Charalambakis, N., (eds), Multiscale Modeling Approaches for Composites: Elsevier, pp. 299–324 (2022)
48. Lemaitre, J.: Coupled elasto-plasticity and damage constitutive equations. Comput. Methods Appl. Mech. Eng. **51**, 31–49 (1985)
49. Detrez, F., Cantournet, S., Seguela, R.: Plasticity/damage coupling in semi-crystalline polymers prior to yielding: micromechanisms and damage law identification. Polymer **52**, 1998–2008 (2011)

50. Krairi, A., Doghri, I.: A thermodynamically-based constitutive model for thermoplastic polymers coupling viscoelasticity, viscoplasticity and ductile damage. Int. J. Plast **60**, 163–181 (2014)